Check for updates

Clinical Science (2019) **133** 2463–2479
https://doi.org/10.1042/CS20190715

PORTLAND PRESS

Research Article

A novel circFMN2 promotes tumor proliferation in CRC by regulating the miR-1182/hTERT signaling pathways

Yongchao Li[1], Changfeng Li[2], Ruisi Xu[2], Yun Wang[3], Dandan Li[2] and Bin Zhang[2]

[1]Department of Gastrointestinal Colorectal Surgery, China-Japan Union Hospital of Jilin University, Changchun 130033, Jilin, P.R. China; [2]Department of Endoscopy Center, China-Japan Union Hospital of Jilin University, Changchun 130033, Jilin, P.R. China; [3]Department of Medicine, Liver and biliary disease Hospital of Jilin province, Changchun 130033, Jilin, P.R. China

Correspondence: Changfeng Li (zhangtang1619@163.com)

OPEN ACCESS

Background: Circular RNAs (circRNAs) are a class of non-coding RNAs broadly expressed in cells of various species. However, the molecular mechanisms that link circRNAs with colorectal cancer (CRC) are not well understood. In the present study, we attempted to provide novel basis for targeted therapy for CRC from the aspect of circRNA–microRNA (miRNA)–mRNA interaction.
Methods: We investigated the expression of circRNAs in five paired CRC tissues and adjacent non-tumor tissues by microarray analysis. Differentially expressed circRNAs were identified between CRC tissues and non-cancerous matched tissues. We focused on hsa_circ_0005100, which is located on chromosome 1 and derived from FMN2, and thus we named it as circFMN2. The expression of circFMN2 was detected in 88 CRC tissues and cell lines by quantitative real-time PCR. Functional assays were performed to evaluate the effects of circFMN2 on proliferation *in vitro*, and on tumorigenesis *in vivo*. The relationship between circFMN2 and miR-1182 was confirmed by luciferase reporter assay.
Results: circFMN2 was found to be significantly up-regulated in CRC tissues and cell lines. Moreover, knockdown of circFMN2 significantly inhibited cell proliferation and migration *in vitro*. Bioinformatics analysis predicted that there is a circFMN2/miR-1182/hTERT axis in CRC progression. Dual-luciferase reporter system validated the direct interaction of circFMN2, miR-1182, hTERT. Western blot verified that inhibition of circFMN2 decreased hTERT expression. Importantly, we demonstrated that circFMN2 was up-regulated in serum exosomes from CRC patients.
Conclusion: In conclusion, circFMN2 is a central component linking circRNAs to progression of CRC via an miR-1182/hTERT axis.

Downloaded from http://portlandpress.com/clinsci/article-pdf/133/24/2463/864387/cs-2019-0715.pdf by guest on 20 August 2022

Introduction

Colorectal cancer (CRC) remains one of the most common and deadly cancers [1]. The incidence of CRC has increased in the last 20 years [2]. Despite considerable progress made in the diagnosis and therapy of this disease, the mortality of CRC is still high [3,4]. Therefore, the underlying mechanisms of CRC progression need to be further elucidated.

Circular RNAs (circRNAs) are a novel class of endogenous RNAs that have a covalent closed loop structure [5]. It is highly evolutionarily conserved and stable and particularly resistant to RNases activity [6]. Growing evidence has indicated that circRNAs are widely involved in diverse physiological and pathological processes, especially in the generation and development of tumors [7–10]. It is reported that circRNAs act as a microRNA (miRNA) sponge which absorbs miRNAs and then regulates the expression of miRNA

Received: 17 July 2019
Revised: 31 October 2019
Accepted: 18 November 2019

Accepted Manuscript online: 18 November 2019
Version of Record published: 20 December 2019

© 2019 The Author(s). This is an open access article published by Portland Press Limited on behalf of the Biochemical Society and distributed under the Creative Commons Attribution License 4.0 (CC BY-NC-ND).

Clinical Science (2019) **133** 2463–2479
https://doi.org/10.1042/CS20190715

targeted genes [11]. In addition, the inherent stability of circRNAs conferred by the circular structure allows them to be enriched in the exosomes and stably present in plasma, saliva and other peripheral tissues, which renders them potential diagnostic molecular markers for various diseases [12–15].

Exosomes are small membrane-derived vesicles with a diameter of approximately 30–150 nm [16]. It has been well established that exosomes originate from multivesicular endosomes (multivesicular bodies) by inverse budding to form multivesicular bodies, and are released into the extracellular space when the multivesicular body fuses with cell membrane exosomes [17]. Exosomes can regulate the physiological and pathological functions of various cancers as message transmitters in intercellular communication because they contain a variety of proteins, lipids, circRNAs, and microRNAs [18]. Recent studies have demonstrated that circRNAs are abundant and stable in exosomes, however, there is little evidence for the expression profile and potential function of secreted circRNAs in CRC.

In the present study, we compared the expression patterns of circRNAs between CRC patients and controls. We identified 448 significantly dysregulated circRNAs in CRC tissues. We focused on hsa_circ_0005100, which is located on chromosome 1 and derived from FMN2, and thus we named it as circFMN2. We further tested circFMN2 in 58 pairs of CRC samples by qRT-PCR and the results showed that the expression of circFMN2 was markedly elevated both in CRC tissues and exosomes from CRC plasma. Silencing circFMN2 suppressed CRC cell growth both *in vitro* and *in vivo*. In mechanism, circFMN2 served as a sponge for miR-1182 promoting CRC progression. Thus, we suggested that circFMN2 might act as an effective therapeutic target for the treatment of CRC. Our findings will provide new insights into the regulatory mechanisms of circFMN2 in CRC progression.

Materials and methods

Tissue specimens

The study was approved by the Clinical Research Ethics Committee of China-Japan Union Hospital of Jilin University and written informed consent was obtained from all the patients. The paired tissue samples were obtained from surgical specimens at the Department of Endoscopy Center, China-Japan Union Hospital of Jilin University. The samples were freshly frozen in liquid nitrogen and stored at −80°C. A total of 62 CRC tissues and adjacent normal colorectal tissues were included in the study. For exosome purification, whole blood samples were collected from these 62 CRC patients and healthy controls. Fresh plasma samples (3 ml) were collected in ethylenediamine tetraacetic acid tubes from each of the subjects. These samples were centrifuged at 3000×***g*** for 10 min at 4°C and then stored at −80°C.

Agilent methods for ceRNA array

Total RNA of exosomes was extracted from plasma using TRIzol LS reagent (Invitrogen, Carlsbad, CA) according to the manufacturer's instructions and quantified using a NanoDrop ND-2000 spectrophotometer (Thermo Fisher Scientific, Wilmington, DE). Total RNA from exosomes were isolated using TRIzol reagent (Invitrogen, Carlsbad, CA) according to the manufacturer's instructions and purified using an RNeasy Mini Kit (Qiagen GmBH, Hilden, Germany). RNA samples of each group were then used to generate fluorescently labeled cRNA targets for the human ceRNA array V1.0 (4× 180 K; Shanghai Biotechnology Corporation, Shanghai, China). The labeled cRNA targets were then hybridized with the slides. After hybridization, slides were scanned on the Agilent Microarray Scanner (Agilent Technologies, Inc., Santa Clara, CA). Data was extracted using Feature Extraction software 10.7 (Agilent Technologies, Inc.). Raw data was normalized by the quantile algorithm of the Limma package in the R program. Microarray experiments were performed at Shanghai Biotechnology Corporation following the protocol of Agilent Technologies, Inc. Ratios between CRC and normal subjects (NC) were calculated. Genes with a fold change (FC) of at least 2 were selected for further analysis. The selected parent genes of circRNA were grouped into functional categories based on the Gene Ontology database (http://www.geneontology.org/) and functional pathways (Kyoto Encyclopedia of Genes and Genomes) were also analyzed using the online enrichment analysis tool of Shanghai Biotechnology Corporation.

The Cancer Genome Atlas dataset analysis

The data and the corresponding clinical information of patients were collected from the Cancer Genome Atlas (TCGA) database (http://cancergenome.nih.gov/). We used the edgeR package of R packages to perform the difference analysis (http://www.bioconductor.org/packages/release/bioc/html/edgeR.html) and used the pheatmap package of R packages to perform the cluster analysis (https://cran.r-project.org/web/packages/pheatmap/index.html). Sva R package was used to remove the batch effect. Genes with adjusted P-values <0.05 and absolute FCs > 1.5 were considered as differentially expressed genes. Kaplan–Meier survival curves were drawn to analyze the relationships

© 2019 The Author(s). This is an open access article published by Portland Press Limited on behalf of the Biochemical Society and distributed under the Creative Commons Attribution License 4.0 (CC BY-NC-ND).

Downloaded from http://portlandpress.com/clinsci/article-pdf/133/24/2463/864387/cs-2019-0715.pdf by guest on 20 August 2022

between genes and overall survival in the survival package. The corresponding statistical analysis and graphics were performed in R software (R version 3.3.2).

Cell lines and culture conditions

The human CRC cell lines (HCT116, DLD1, SW480, RKO, HT-29) were purchased from the Institute of Biochemistry and Cell Biology of the Chinese Academy of Sciences (Shanghai, China). The human colonic epithelial cell line HCoEpiC and the 293T cell line were obtained from American Type Culture Collection (Manassas, VA). Cells were cultured in RPMI 1640 or DMEM (Gibco, Grand Island, NY, U.S.A.) supplemented with 10% fetal bovine serum (10% FBS), 100 U/ml penicillin, and 100 mg/ml streptomycin (Gibco) in humidified air at 37°C with 5% CO_2.

RNA extraction and qRT-PCR

TRIzol Reagent (Invitrogen) was used to extract total RNA from tissues. For circRNAs, RNase R was used to degrade linear RNA, which have poly (A), and amplified by divergent primer. qRT-PCR analysis on circRNA and mRNA was performed using Prime Script RT reagent Kit (TaKaRa) and SYBR Premix Ex Taq II (TaKaRa). The b-actin was used as an endogenous control. For miR-1182 analysis, miRNA was treated with DNase I to eliminate genomic DNA and cDNA was synthesized by Mir-X miR First-Strand Synthesis Kit (TaKaRa). SYBR Premix Ex Taq II (TaKaRa) was used for qRT-PCR. The expression was normalized to RNU6-2. The $2^{-\Delta\Delta C_t}$ method was adopted to calculate relative expression of circFMN2 and hsa-miR-1182.

Cell transfection

Small interfering RNAs (siRNAs) targeting the back-splice junction sequences of circFMN2 and the respective negative control oligonucleotides were synthesized by GenePharma (Shanghai, China). The siRNA sequences: si-circFMN2#1: AGACTTGAAAGCTGTTGTGAA, si-circFMN2#2: AAGACTTGAAAGCTGTTGTGA, and si-circFMN2#3: AAGAAAGACTTGAAAGCTGTT. A pcDNA 3.1 circRNA mini vector was used to ectopically express circFMN2 level in CRC cells. The miR-1182 mimics, inhibitor and NC were synthesized from GenePharma (Shanghai, China). We used Lipofectamine 3000 for transfection following the protocols of the manufacturer.

Cell counting kit-8 and colony formation assay

Cell proliferation rates were detected with Cell Counting Kit-8 (CCK-8, Dojindo, Japan). A total of 2×10^3 cells were cultured in each 96-well plate and the absorbance at 450 nm was measured after incubation with 10 μl CCK-8 solution at 37°C for 1 h. Cells (500 per well) were seeded in six-well plates for 1–2 weeks. The colonies were stained with 0.1% Crystal Violet solution diluted by anhydrous methanol for 15 min. Colonies were microscopically examined and counted. All detections were carried out in triplicate.

Cell cycle analysis

Cells for cell cycle analysis were stained with Propidium Oxide by the CycleTEST PLUS DNA Reagent Kit (BD Biosciences) following the protocol and were analyzed by FACScan. The percentage of the cells in G_0–G_1, S, and G_2–M phase were counted and compared.

Apoptosis analysis

Cell apoptosis was analyzed using the Annexin V-FITC Apoptosis Detection Kit (KeyGen Biotech, Nanjing, China) according to the manufacturer's instructions. Forty-eight hours after transfection, cells were stained with FITC and Propidium Iodide. Then flow cytometry was performed using a FACS Canto II (BD Biosciences) and the data were analyzed using BD FCSDiva Software and FCS Express 5 software (De Novo Software, Los Angeles, CA).

Immunohistochemistry

For each patient sample, three paraffin sections of 5 μm were prepared, one for Hematoxylin and Eosin (HE) staining and the other two for immunohistochemical staining. Phosphate-buffered saline (PBS) instead of primary antibodies was used for negative control, and the breast cancer tissue was used for positive control. Sections were dewaxed using xylene, followed by hydration with ethanol solutions, and addition of EDTA for antigen retrieval. Later, sections were blocked with normal goat serum for 30 min to eliminate non-specific binding. Sections were incubated with anti-human FMN2 polyclonal antibody (1:300; ab72052, Abcam Inc., Cambridge, MA, U.S.A.) and and anti-human hTERT polyclonal antibody (1:100; ab183105, Abcam Inc., Cambridge, MA, U.S.A.). Sections were then incubated

Downloaded from http://portlandpress.com/clinsci/article-pdf/133/24/2463/864387/cs-2019-0715.pdf by guest on 20 August 2022

© 2019 The Author(s). This is an open access article published by Portland Press Limited on behalf of the Biochemical Society and distributed under the Creative Commons Attribution License 4.0 (CC BY-NC-ND).

Clinical Science (2019) **133** 2463–2479
https://doi.org/10.1042/CS20190715

with biotin-labeled secondary antibodies for 30 min at room temperature, followed by staining with diaminobenzidine (DAB). Finally, the sections were counterstained with Hematoxylin. The result of staining was determined by two doctors who did not know the clinical condition of patients. The proportions of positive cells of 0, 1–5, 6–25, 26–75, and 76–100% were assigned the scores of 0, 1, 2, 3, and 4, respectively. Scores of 0–2 were considered as negative expression, and scores of 3–4 were considered as positive expression.

Xenografts in mice

Approximately 1×10^6 cells were injected subcutaneously into the right neck of male BALB/C nude mice (age, 4–6 weeks; weight, 18–22 g, five mice per group) purchased from Slaccas (Slaccas Laboratory Animal, Shanghai, China). The length and width of tumor xenografts were measured weekly by Vernier calipers, and the tumor volume was calculated using the following formula: Volume (mm^3) $= 0.5 \times \text{width}^2 \times \text{length}$. Six weeks after injection, the mice were killed by cervical dislocation. The animal studies were conducted in accordance with the ethical guidelines for animal experiment and approved by the Animal Care and Use Committee of the China-Japan Union Hospital of Jilin University. The animal work took place in the animal central of China-Japan Union Hospital of Jilin University.

Luciferase reporter assay

The recombination luciferase plasmids containing circFMN2 full-length sequences with wild-type or mutant miR-1182 binding site were constructed from Genecopoeia company (Rockville, MD, U.S.A.). Subsequently, luciferase plasmids were co-transfected with control or miR-1182 mimics into cells by Lipofectamine 3000 (Invitrogen). After 48 h of treatment, the luciferase activity in each group was measured by using a dual luciferase reporter assay system (Promega, Madison, WI, U.S.A.).

RNA immunoprecipitation assay

RNA immunoprecipitation (RIP) assay was performed using an EZ-Magna RiP Kit (Millipore, Billerica, MA, U.S.A.) in accordance with the manufacturer's instructions. Cells were lysed at 70–80% confluence in RIP lysis buffer, and then incubated with magnetic beads conjugated with human anti-Ago2 antibody (Millipore) and normal mouse IgG control (Millipore) in RIP buffer. The RNAs in the immunoprecipitates were isolated with TRIzol reagent and analyzed by qRT-PCR.

Plasma exosome isolation

First, the samples were centrifuged twice at $3000\times\boldsymbol{g}$ and $10000\times\boldsymbol{g}$ for 20 min at room temperature to remove cells and other debris in the plasma. The supernatants were then centrifuged at $100000\times\boldsymbol{g}$ for 30 min at 4°C to remove microvesicles that were larger than exosomes, harvested, and again centrifuged at $10000\times\boldsymbol{g}$ for 70 min at 4°C. Subsequently, the supernatants were gently decanted, and the exosome sediments were re-suspended in PBS. Concentration of exosomes was determined using BCA method as recommended by the manufacturer (Thermo Scientific, U.S.A.).

Transmission electron microscopy

The exosome suspension was diluted to 0.5 mg/ml with PBS, and then spotted on to a glow-discharged copper grid placed on a filter paper and dried for 10 min by exposure to infrared light. Next, the exosome samples were stained with one drop of phosphotungstic acid (1% aqueous solution) for 5 min and dried for 20 min by exposure to infrared light. Finally, the exosomes were visualized under a transmission electron microscope (HT7700, Hitachi, Tokyo, Japan) at 100 keV.

Nanoparticle tracking analysis

Briefly, the exosomes were resuspended in PBS and filtered with a syringe filter (Millipore). Then, the samples were diluted until individual nanoparticles could be tracked. The size distribution of the exosomes was evaluated using a NanoSight NS300 instrument (Malvern Instruments Ltd, Worcestershire, U.K.).

Western blot assay

The lysates from cells were collected by RIPA buffers (Beyotime Biotechnology, Shanghai, China) and then boiled for 5 min at 100°C. After that, the proteins were transferred to PVDF membrane and blocked by non-fat dried milk. The membrane was incubated with primary antibodies at 4°C overnight. The next day, the membrane was washed strictly and probed with HRP–conjugated secondary antibody, followed by visualization with ECL Plus chemiluminescence reagent (Beyotime Biotechnology).

© 2019 The Author(s). This is an open access article published by Portland Press Limited on behalf of the Biochemical Society and distributed under the Creative Commons Attribution License 4.0 (CC BY-NC-ND).

Downloaded from http://portlandpress.com/clinsci/article-pdf/133/24/2463/864387/cs-2019-0715.pdf by guest on 20 August 2022

PORTLAND PRESS

Statistical analysis

All statistical analyses were performed by SPSS 19.0 software. The differences between two groups were calculated using Student's *t* or Chi-square test. Survival data were evaluated using the Kaplan–Meier method and log-rank test. $P<0.05$ was considered statistically significant.

Results

Profiles of circRNAs in CRC

A total of 11245 circRNAs were detected in CRC and paired non-tumorous samples by the circRNA microarray analysis. Among them, 1075 circRNAs were significantly aberrantly expressed ($P<0.05$ and fold-change > 2.0) between CRC tissues and paired non-tumorous tissues. Of these circRNAs, 558 were significantly up-regulated and 517 were significantly down-regulated in CRC tissues compared with paired adjacent normal tissues. Hierarchical clustering was then performed to demonstrate the five most up-regulated circRNAs (hsa_circ_0005100, hsa_circ_0001821, hsa_circ_0084188, hsa_circ_0000372, and hsa_circ_0001178) and five most down-regulated circRNAs (hsa_circ_0000374, hsa_circ_0036592, hsa_circ_0006271, hsa_circ_0009155, and hsa_circ_0002211) expression patterns among the sets (Figure 1A).

The five most up-regulated circRNAs were selected and validated by qRT-PCR using 88 CRC and paired non-tumorous tissue samples. As shown in Figure 1B–F, except for hsa_circ_0000372, the circRNAs displayed a consistent expression level between the microarray and qRT-PCR analyses. There was an increasing trend in hsa_circ_0005100 (chr1:240458121-240497529) levels from non-tumorous tissues to CRC tissues, with more than 10 FC from microarray analysis. By browsing the human reference genome (GRCh37/hg19), we identified that hsa_circ_0005100 is derived from FMN2, which is located on chromosome 1, with a spliced mature sequence length of 612 base pairs (bp), and thus we named it as circFMN2.

To further investigate the role of circFMN2 in CRC, the relationship between circFMN2 expression in CRC tissues and clinicopathological characteristics of CRC patients was analyzed. Using the median expression level of circFMN2 as cut-off value, patients who expressed circFMN2 equal to or greater than the average level were assigned to the 'circFMN2 high' group. As shown in Table 1, high expression of circFMN2 in CRC tissues was significantly correlated with larger tumor size ($P=0.012$), advanced tumor stage ($P=0.011$), distant metastasis ($P=0.001$), and TNM stage ($P=0.03$), but not with other characteristics of CRC that included age ($P=0.521$), gender ($P=0.286$), lymph node metastasis ($P=0.829$), or histological grade ($P=0.134$). The data provide evidence of the importance of circFMN2 in the growth and tumorigenesis of CRC.

Knockdown of circFMN2 inhibits CRC growth *in vitro*

The expression level of circFMN2 in multiple CRC and a normal colonic epithelial cell (HCoEpiC) were measured. The expression level of circFMN2 in CRC cell lines was generally higher than that in the HCoEpiC normal colonic cell line (Figure 2A; $P<0.01$). The expression of circFMN2 was highest in HCT116 cells and lowest in HT-29 cells. Using the backsplice junction-specific siRNA (respectively si-circFMN2#1, si-circFMN2#2, or si-circFMN2#3), we successfully knocked down circFMN2 expression in HCT116 cells (Figure 2B; $P<0.01$). The si-circFMN2#3 was used in the following experiments. Using circFMN2-overexpressing lentivirus, the circFMN2 expression in HT-29 cells was shown to be dramatically increased (Figure 2C).

Analyses using CCK-8 (Figure 2D,E; $P<0.01$) and colony formation (Figure 2F) revealed that the knockdown of circFMN2 significantly restrained the proliferation of HCT116 cells, while ectopic expression of circFMN2 significantly promoted the proliferation of HT-29 cells. However, CCK-8 assay revealed that the knockdown of circFMN2 did not inhibit the proliferation of HCoEpiC cells, and ectopic expression of circFMN2 did not promote the proliferation of HCoEpiC cells (Supplementary Figure S1A,B). We further investigated whether circFMN2 affected cell cycle progression or apoptosis of CRC cells using flow cytometry. The knockdown of circFMN2 significantly increased the percent of HCT116 cells in G_0/G_1 phase and decreased the percent of HCT116 cells in G_2/M phase. The overexpression of circFMN2 significantly decreased the percent of HT-29 cells in G_0/G_1 phase and increased the percent of HT-29 cells in G_2/M phase (Figure 3A,B; $P<0.01$). However, circFMN2 overexpression and knockdown did not affect apoptosis of CRC cells (Figure 3C,D). The collective findings suggested that knockdown of circFMN2 inhibits the proliferation of CRC cells by facilitating DNA synthesis.

CircFMN2 has no effect on its linear transcript

Some circRNAs regulate the expression and function of the corresponding linear transcripts. Therefore, the regulatory relationship between circFMN2 and its linear transcript (FMN2) was investigated in the present study. We first

Downloaded from http://portlandpress.com/clinsci/article-pdf/133/24/2463/864387/cs-2019-0715.pdf by guest on 20 August 2022

© 2019 The Author(s). This is an open access article published by Portland Press Limited on behalf of the Biochemical Society and distributed under the Creative Commons Attribution License 4.0 (CC BY-NC-ND).

Clinical Science (2019) **133** 2463–2479
https://doi.org/10.1042/CS20190715

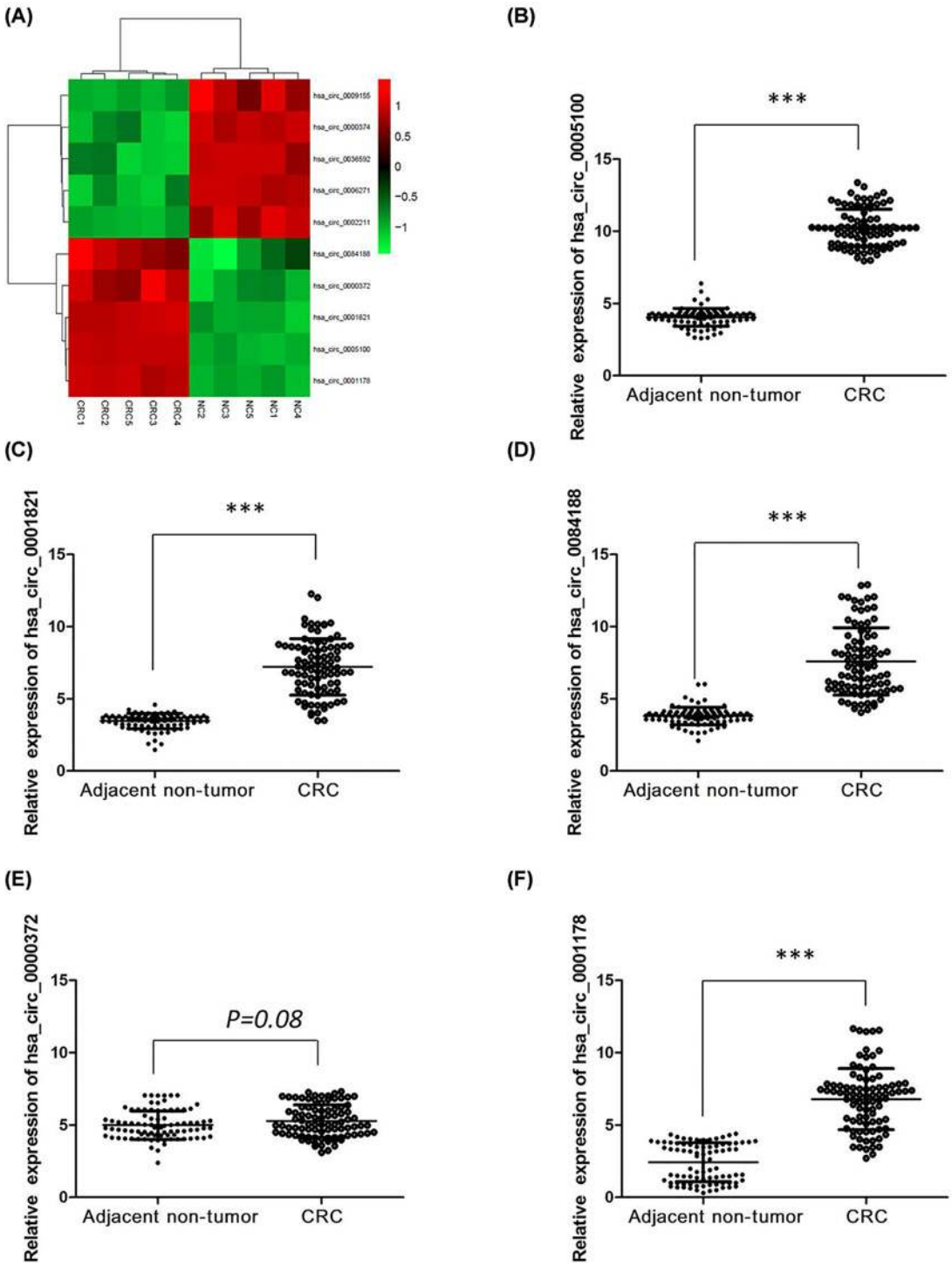

Figure 1. Deregulated circRNAs in CRC tumor tissues

(**A**) The heat map showed the top ten most increased and decreased circRNAs in CRC tissues as compared with that in the matched non-tumor tissues analyzed by circRNAs Arraystar Chip. (**B**) The level of hsa_circ_0005100 was significantly increased in tumor tissues as compared with that in matched non-tumor tissues of 88 pairs of CRC patients. (**C**) The level of hsa_circ_0001821 was significantly increased in tumor tissues as compared with that in matched non-tumor tissues of 88 pairs of CRC patients. (**D**) The level of hsa_circ_0084188 was significantly increased in tumor tissues as compared with that in matched non-tumor tissues of 88 pairs of CRC patients. (**E**) The level of hsa_circ_0000372 was not significantly increased in tumor tissues as compared with that in matched non-tumor tissues of 88 pairs of CRC patients; P=0.09. (**F**) The level of hsa_circ_0001178 was significantly increased in tumor tissues as compared with that in matched non-tumor tissues of 88 pairs of CRC patients. ***P<0.001.

© 2019 The Author(s). This is an open access article published by Portland Press Limited on behalf of the Biochemical Society and distributed under the Creative Commons Attribution License 4.0 (CC BY-NC-ND).

Downloaded from http://portlandpress.com/clinsci/article-pdf/133/24/2463/864387/cs-2019-0715.pdf by guest on 20 August 2022

Table 1 Correlation between circFMN2 expression and clinicopathologic characteristics of CRC patients

Clinicopathological features	Overall (*n*=88)	circFMN2		*P*
		High (*n*=44)	Low (*n*=44)	
Age				
<60	48	26	22	0.521
≥60	40	18	22	
Gender				
Male	46	20	26	0.286
Female	42	24	18	
Tumor size				
>5 cm	30	21	9	0.012
≤5 cm	58	23	35	
Tumor stage				
T1 and T2	60	24	36	0.011
T3 and T4	28	20	8	
Lymph node metastasis				
N1–2	38	20	18	0.829
N0	50	24	26	
Distant metastasis				
Absent	66	26	40	0.001
Present	22	18	4	
TNM stage				
I/II	62	26	36	0.03
III/IV	26	18	8	
Histological grade				
Well/moderately	48	20	28	0.134
Poorly	40	24	16	

analyzed the colon adenocarcinoma (COAD) dataset from the TCGA database and found that the level of FMN2 was significantly lower in 275 COAD tissues than 349 normal tissues ($P<0.05$; Figure 4A). However, Kaplan–Meier survival analysis from TCGA COAD datasets suggested that FMN2 expression is not significantly associated with worse overall survival (OS) (log-rank test, $P=0.69$, Figure 4B) and disease-free survival (DFS) of COAD patients (log-rank test, $P=0.26$, Figure 4C). Moreover, we used IHC assay to analyze the expression of FMN2 in our cohort of 88 pairs of CRC tumor tissues. FMN2 was significantly down-regulated in CRC tissues compared with adjacent non-tumorous tissues (Figure 4D). FMN2 did not change in both mRNA and protein levels when the expression of circFMN2 was artificially changed in CRC cells (Figure 4E,F and Supplementary Figure S1C,D). These data indicated that FMN2 is not the target gene of circFMN2.

CircFMN2 promoted CRC progression by sponging miR-1182

Increasing studies have verified that circRNAs can exert their functions by acting as ceRNAs to sponge miRNAs [16–18]. Considering the cytoplasmic localization of circFMN2 in CRC cells, we investigated whether circFMN2 exerted function in CRC in an miRNA-mRNA-dependent manner. Therefore, we used the StarBase v2.0 target prediction tool to find 28 potential miRNAs that could bind to circFMN2 (Supplementary Data S1). To figure out the miRNA implicated in CRC, all candidate miRNAs were subjected to microarray analysis. Among them, ten miRNAs were significantly down-regulated in response to circFMN2 overexpression (Figure 5A). For further selection, we chose top five down-regulated miRNAs to do circRIP assay. The results demonstrated the interaction of only miR-1182 with circFMN2 (Figure 5B; $P<0.01$). To validate the interaction between circFMN2 and miR-1182, we obtained the binding sequence between miR-1182 and circFMN2 (Figure 5C). Next, luciferase reporter assays were carried out to verify whether there was a direct interaction between circFMN2 and miR-1182. As shown in Figure 5D, miR-1182 mimics could significantly decrease the luciferase activity of the vector containing the wild-type miR-1182 binding site within circFMN2 in HCT116 cells, while the luciferase activity of the vector containing the mutant binding site was restored. In a further RIP experiment, circFMN2 and miR-1182 simultaneously existed in the production precipitated by anti-AGO2 (Figure 5E; $P<0.01$), suggesting that miR-1182 is circFMN2-targeting miRNA. These outcomes indicated that the interaction of circFMN2 and miR-1182 was realized by the putative binding site.

© 2019 The Author(s). This is an open access article published by Portland Press Limited on behalf of the Biochemical Society and distributed under the Creative Commons Attribution License 4.0 (CC BY-NC-ND).

Downloaded from http://portlandpress.com/clinsci/article-pdf/133/24/2463/864387/cs-2019-0715.pdf by guest on 20 August 2022

Clinical Science (2019) **133** 2463–2479
https://doi.org/10.1042/CS20190715

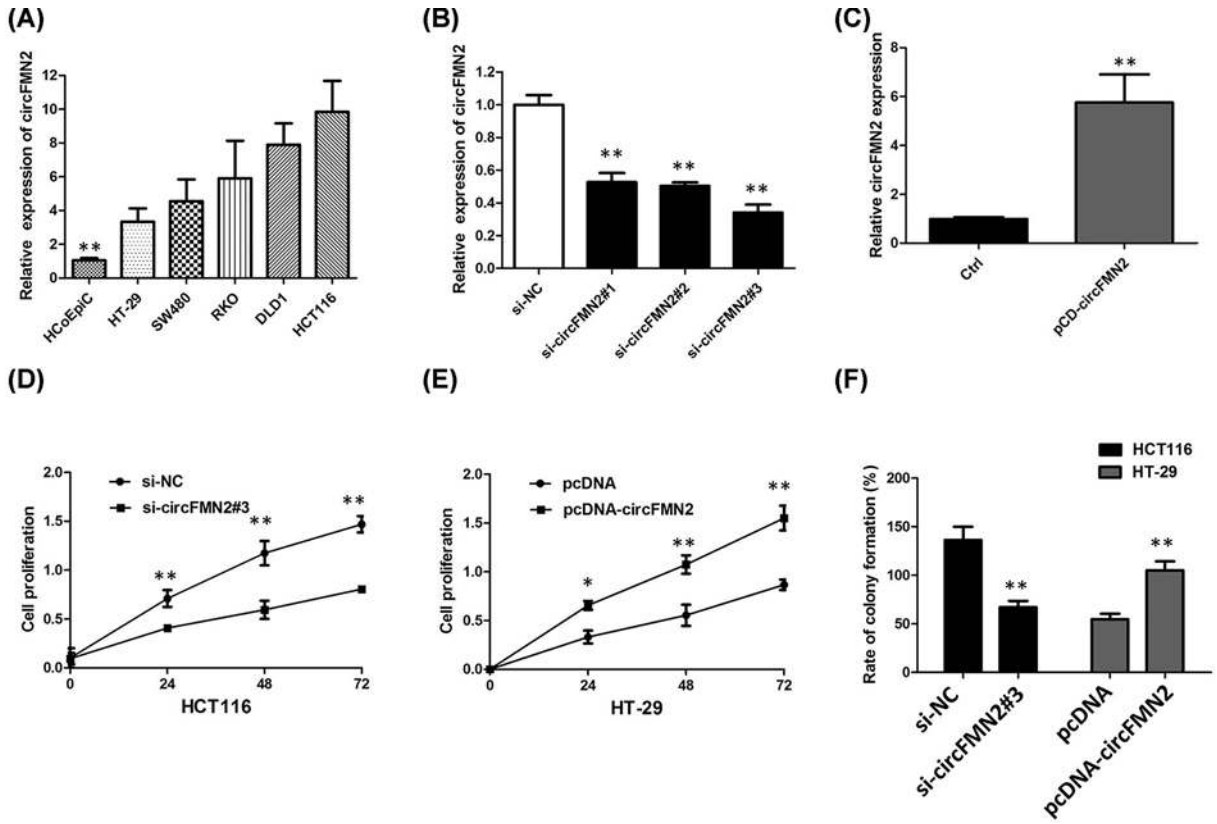

Figure 2. Knockdown of circFMN2 inhibits CRC growth *in vitro*

(**A**) The qRT-PCR assay indicated the expression level of circFMN2 in CRC cell lines was generally higher than that in the HCoEpiC normal colonic cell line. (**B**) The qRT-PCR assay indicated the expression level of circFMN2 in HCT116 cells treated with si-circFMN2. Data are the mean ± SD of three experiments. (**C**) The qRT-PCR assay indicated the expression level of circFMN2 in HT-29 cells infected with circFMN2 overexpression plasmid. (**D**) CCK8 assay showed that circFMN2 knockdown significantly repressed cell proliferation of HCT116 cells. (**E**) CCK8 assay showing overexpression of circFMN2 promoted the proliferation of HT-29 cells. (**F**) Colony formation assay showed that the knockdown of circFMN2 significantly restrained the proliferation of HCT116 cells, while ectopic expression of circFMN2 significantly promoted the proliferation of HT-29 cells. *$P<0.05$, **$P<0.01$.

The qRT-PCR analysis indicated that miR-1182 was expressed at low level in CRC tissues (Supplementary Figure S2A; $P<0.01$). The expression of miR-1182 was obviously decreased in HCT116 cells, indicating the opposite result to circFMN2 expression (Supplementary Figure S2B; $P<0.01$). The decreased expression level of miR-1182 in circFMN2-overexpressed CRC cells indicated the negative regulatory effect of circFMN2 on miR-1182 expression (Figure 4F and Supplementary Figure S2C; $P<0.01$). Furthermore, miR-1182 had the similar tumor-suppressing effects as circFMN2 silencing (Figure 5G and Supplementary Figure S2D; $P<0.01$). These data suggested that circFMN2 might exert its functions by sponging miR-1182 in CRC.

CircFMN2 up-regulates hTERT expression via sponging miR-1182

Previous studies have reported that several genes are directly targeted by miR-1182 in human cancers including hTERT, SKA1, and CDK14 [19–21]. However, we did not detect significant changes in the expression levels of these mRNAs in HCT116 cells transfected with an miR-1182 mimic or in HT-29 cells transfected with an miR-1182 inhibitor except for the expression of the hTERT (Figure 6A,B; $P<0.01$). TargetScan online software demonstrated that hTERT was a candidate target of miR-1182 (Figure 6C). To verify whether the 3′ UTR of hTERT mRNA was a target of miR-1182 in 293T cells, a luciferase reporter gene assay was used. The wild-type (wt) 3′ UTR sequence or mutant (mu) 3′ UTR sequence of hTERT was cloned into a luciferase reporter vector. The luciferase activity was significantly inhibited by the miR-1182 mimics in wt 3′ UTR sequence-transfected 293T cells. Conversely, the luciferase activity was not inhibited by the miR-1182 mimics in mu 3′ UTR sequence-transfected cells (Figure 6D; $P<0.01$). These findings indicate a direct interaction between miR-1182 and hTERT mRNA in CRC cells. We determined the

© 2019 The Author(s). This is an open access article published by Portland Press Limited on behalf of the Biochemical Society and distributed under the Creative Commons Attribution License 4.0 (CC BY-NC-ND).

Downloaded from http://portlandpress.com/clinsci/article-pdf/133/24/2463/864387/cs-2019-0715.pdf by guest on 20 August 2022

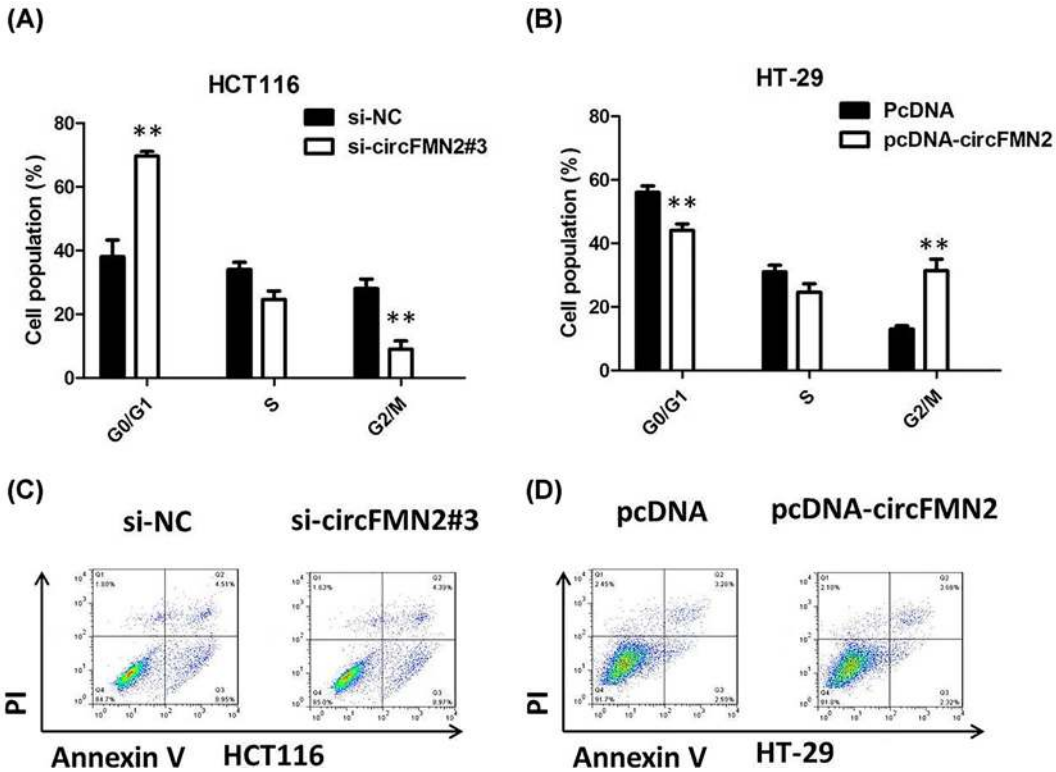

Figure 3. Knockdown of circFMN2 inhibits the proliferation of CRC cells by inducing cell cycle arrest

(**A**) The knockdown of circFMN2 significantly increased the percent of HCT116 cells in G_0/G_1 phase and decreased the percent of HCT116 cells in G_2 phase. Data are the means ± SD of three experiments. (**B**) The overexpression of circFMN2 significantly decreased the percent of HT-29 cells in G_0/G_1 phase and increased the percent of HT-29 cells in G_2 phase. Data are the means ± SD of three experiments. (**C**) circFMN2 knockdown did not affect apoptosis of HCT116 cells. (**D**) circFMN2 overexpression did not affect apoptosis of HT-29 cells. Data are the means ± SD of three experiments; $^{**}P<0.01$.

expression of hTERT in 88 CRC patient tissues using qRT-PCR and IHC. We also found that hTERT expression was higher in CRC tissues compared with their normal counterparts (Figure 6E,F; $P<0.01$). Then, we found that levels of hTERT were negatively regulated by circFMN2 knockdown, and the effect of inhibition of circFMN2 was attenuated by miR-1182 inhibitor (Figure 6G; $P<0.01$). These data further demonstrated the regulatory network of circFMN2/miR-1182/hTERT. According to above data, we confirmed that circFMN2 can exert function in CRC by sponging miR-1182 to up-regulate hTERT expression.

Knockdown of circFMN2 inhibits CRC growth *in vivo*

HCT116 cells were used to establish a stable CRC cell line with low circFMN2 expression via lentiviral-circFMN2-RNAi. HCT116 cells with low or normal circFMN2 expression induced by transfection with lentiviral or control vectors were subcutaneously implanted into nude mice. Compared with the control group, smaller tumor size and lower tumor weight were observed in the low circFMN2 expression group group (Figure 7A–C, $P<0.01$). IHC staining results showed that knockdown circFMN2 significantly inhibited the expression levels of Ki-67 when compared with the control group (Figure 7D). These results demonstrated that circFMN2 can promote the growth of CRC *in vivo*.

CircFMN2 is secreted by exosomes into serum of CRC patients

Finally, in our current study, we collected abundant serums from 35 CRC patients and 30 normal people. After isolation of serum exosomes by sequential centrifugation, transmission electron microscopy (TEM) analysis showed that isolated CRC-secreted exosomes had similar morphologies (30–150 nm in diameter) and exhibited a round-shaped appearance (Figure 8A). The nanoparticle tracking analysis (NTA) results demonstrated that isolated CRC-secreted exosomes showed a similar size distribution, and the peak size range was 80–135 nm. Moreover, the presence of the

© 2019 The Author(s). This is an open access article published by Portland Press Limited on behalf of the Biochemical Society and distributed under the Creative Commons Attribution License 4.0 (CC BY-NC-ND).

Downloaded from http://portlandpress.com/clinsci/article-pdf/133/24/2463/864387/cs-2019-0715.pdf by guest on 20 August 2022

Clinical Science (2019) **133** 2463–2479
https://doi.org/10.1042/CS20190715

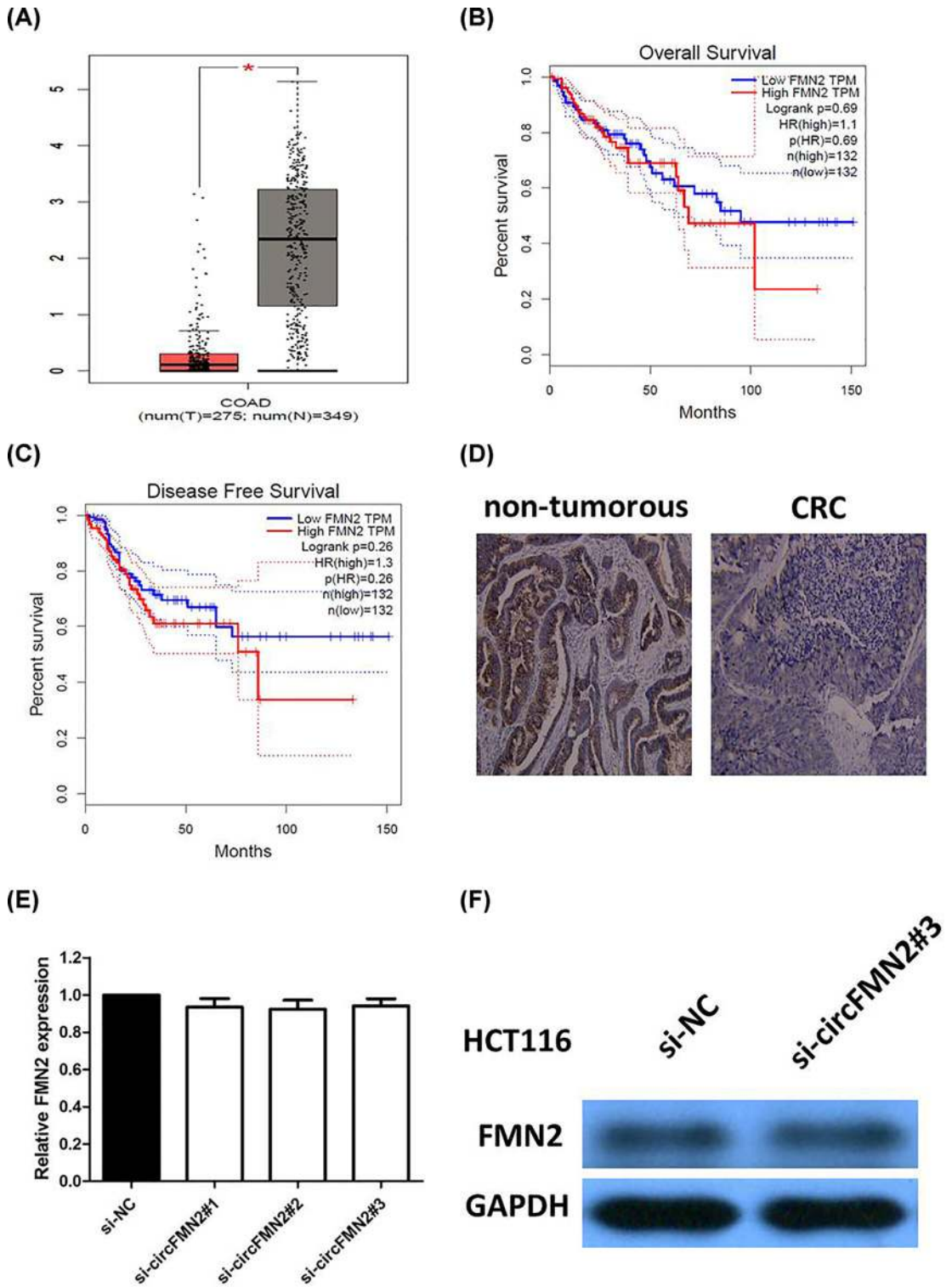

Figure 4. CircFMN2 has no effect on its linear transcript

(**A**) FMN2 expression in CRC and normal samples from the TCGA COAD dataset. (**B**) Kaplan–Meier analyses of the correlations between FMN2 expression and OS of COAD patients from the TCGA COAD dataset. (**C**) Kaplan–Meier analyses of the correlations between FMN2 expression and DFS of COAD patients from the TCGA COAD dataset. (**D**) IHC assay indicated the expression of FMN2 was significantly down-regulated in CRC tissues compared with adjacent non-tumorous tissues. (**E**) The qRT-PCR assay indicated circFMN2 knockdown did not change the mRNA level of FMN2. (**F**) The Western blot assay indicated circFMN2 knockdown did not change the protein level of FMN2. *$P<0.05$.

© 2019 The Author(s). This is an open access article published by Portland Press Limited on behalf of the Biochemical Society and distributed under the Creative Commons Attribution License 4.0 (CC BY-NC-ND).

Downloaded from http://portlandpress.com/clinsci/article-pdf/133/24/2463/864387/cs-2019-0715.pdf by guest on 20 August 2022

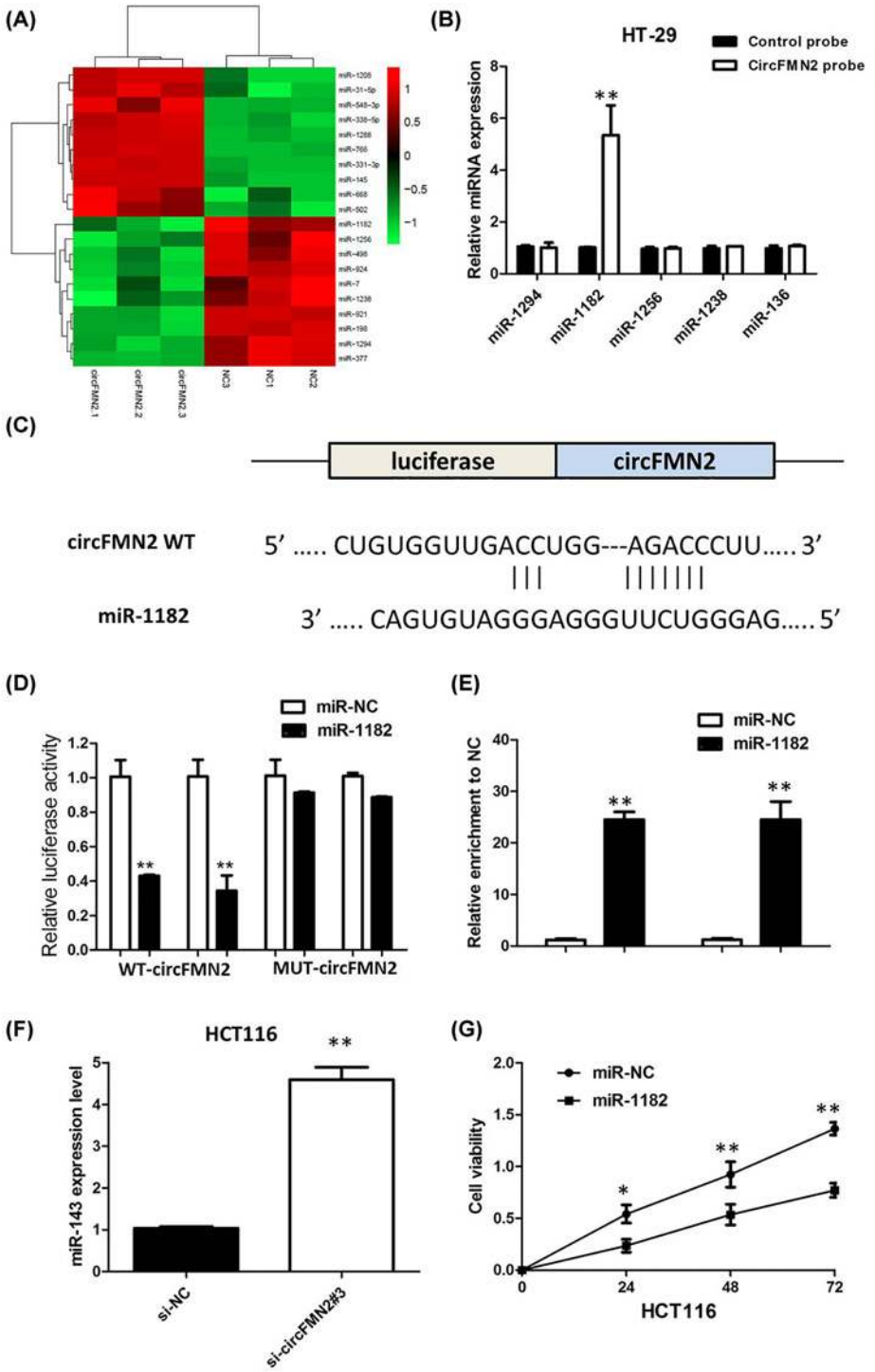

Figure 5. CircFMN2 promoted CRC progression by sponging miR-1182

(**A**) The microarray analysis showed that ten miRNAs were significantly down-regulated in response to circFMN2 overexpression. (**B**) The circRIP assay showed that the interaction of only miR-1182 with circFMN2. (**C**) The binding sequence between miR-1182 and circFMN2. (**D**) Dual luciferase reporter showed significant reduction in luciferase activity of the wild-type and luciferase activity is restored by the mutant sequence. (**E**) The RIP experiment showed that miR-1182 and circFMN2 simultaneously existed in the production precipitated by anti-AGO2. (**F**) Knockdown of circFMN2 increased expression level of miR-1182 in HCT116 cells. (**G**) CCK8 assay showed that miR-1182 mimic significantly inhibited cell proliferation of HCT116 cells. Data are the means ± SD of three experiments; $^{*}P<0.05$, $^{**}P<0.01$.

© 2019 The Author(s). This is an open access article published by Portland Press Limited on behalf of the Biochemical Society and distributed under the Creative Commons Attribution License 4.0 (CC BY-NC-ND).

Downloaded from http://portlandpress.com/clinsci/article-pdf/133/24/2463/864387/cs-2019-0715.pdf by guest on 20 August 2022

Clinical Science (2019) **133** 2463–2479
https://doi.org/10.1042/CS20190715

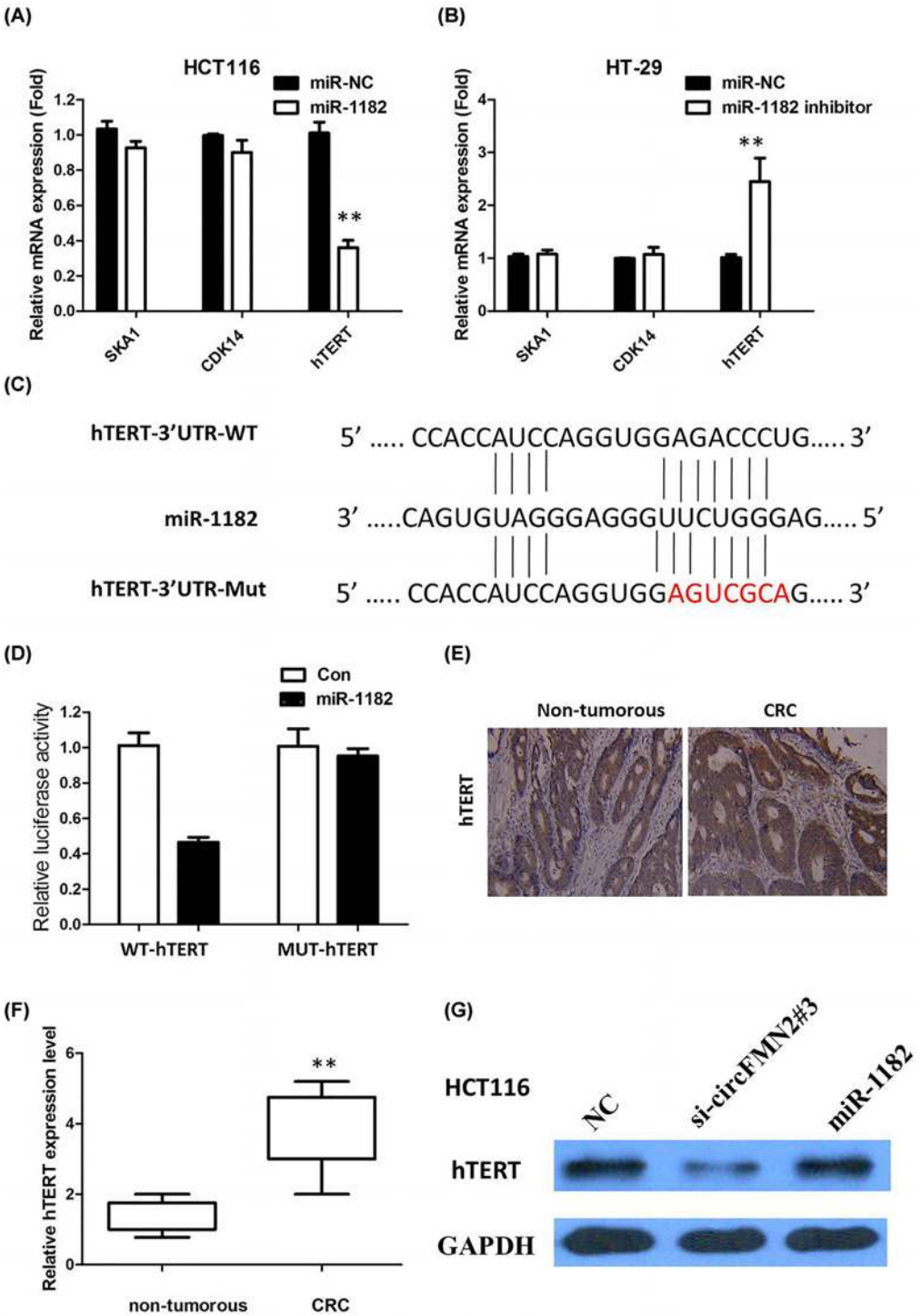

Figure 6. CircFMN2 up-regulates hTERT expression via sponging miR-1182

(**A**) HCT116 cells transfected with an miR-1182 mimic decreased the expression of the hTERT. (**B**) HT-29 cells transfected with an miR-1182 inhibitor increased the expression of the hTERT. (**C**) Bioinformatics analysis revealed the predicted binding sites between hTERT and miR-1182. (**D**) Luciferase reporter assay demonstrated that miR-1182 mimics significantly decreased the luciferase activity of hTERT-wt in 293T cells. (**E**) IHC assay indicated the expression of hTERT was significantly up-regulated in CRC tissues compared with adjacent non-tumorous tissues. (**F**) The qRT-PCR assay indicated the expression level of hTERT was significantly up-regulated in CRC tissues compared with adjacent non-tumorous tissues. (**G**) The effect of knockdown circFMN2 on protein levels of hTERT was attenuated by miR-1182 inhibitor. All tests were at least performed three times. Data were expressed as mean $\pm$ SD; $^{**}P<0.01$.

© 2019 The Author(s). This is an open access article published by Portland Press Limited on behalf of the Biochemical Society and distributed under the Creative Commons Attribution License 4.0 (CC BY-NC-ND).

Downloaded from http://portlandpress.com/clinsci/article-pdf/133/24/2463/864387/cs-2019-0715.pdf by guest on 20 August 2022

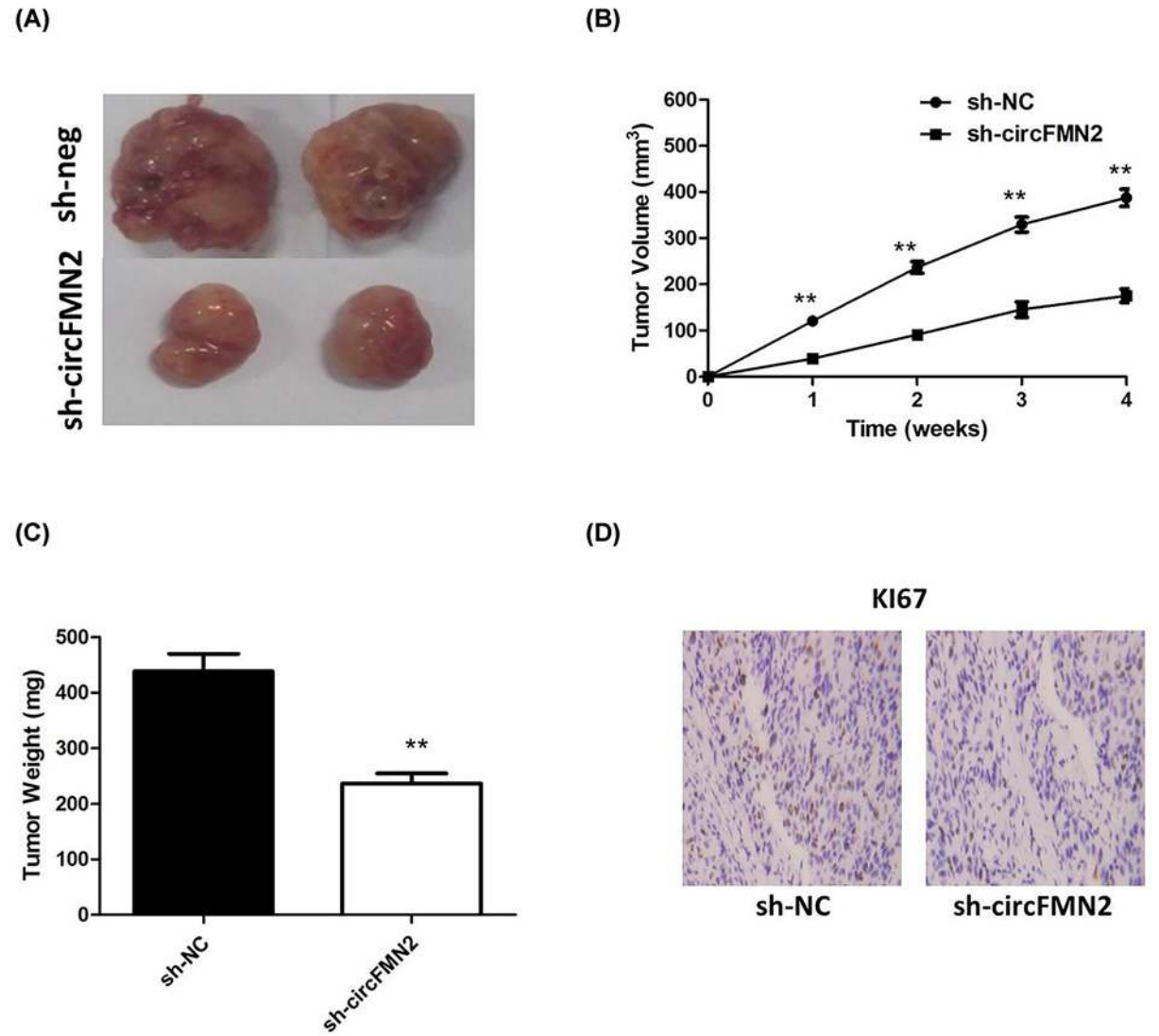

Figure 7. circFMN2 promoted CRC cell growth *in vivo*

(**A**) circFMN2 knockdown inhibits tumor growth *in vivo*. (**B**) The tumor volume curve of nude mice was analyzed. (**C**) The tumor weights of nude mice were measured. (**D**) IHC analysis was performed to examine the expression levels of proliferation marker Ki-67 in tumors of nude mice. Knockdown of circFMN2 significantly decreased the percentage of Ki-67 positive cells in tumors of nude mice compared with that of sh-NC xenografts. $^{**}P<0.01$.

exosome markers CD63, TSG101, and HSP70 were confirmed by Western blot (Figure 8B). Our results showed that circFMN2 expression is detectable in extracted serum exosomes derived from CRC patients (Figure 8C; $P<0.01$). Furthermore, there was a significant inverse correlation between the expression levels of circFMN2 and miR-1182 in serum exosomes derived from CRC patients (Figure 8D, $r = -0.821$, $P<0.0001$).

Discussion

circRNAs are a group of non-coding RNAs that in recent years have emerged as potential regulators of many cell processes [22,23]. Currently, with the development of deep RNA sequencing (RNA-seq) technologies and novel bioinformatics approaches, abundant and diverse circRNAs have been detected and identified, including few circRNA functions, such as regulating transcription in the nucleus, functioning as efficient microRNA sponges, competing with pre-mRNA splicing, and serving as circRNA–protein interactions [24,25]. However, details of the mechanisms of circRNAs in CRC remain ambiguous. Therefore, it is necessary to seek out new biomarkers and explore their

© 2019 The Author(s). This is an open access article published by Portland Press Limited on behalf of the Biochemical Society and distributed under the Creative Commons Attribution License 4.0 (CC BY-NC-ND).

Downloaded from http://portlandpress.com/clinsci/article-pdf/133/24/2463/864387/cs-2019-0715.pdf by guest on 20 August 2022

Clinical Science (2019) **133** 2463–2479
https://doi.org/10.1042/CS20190715

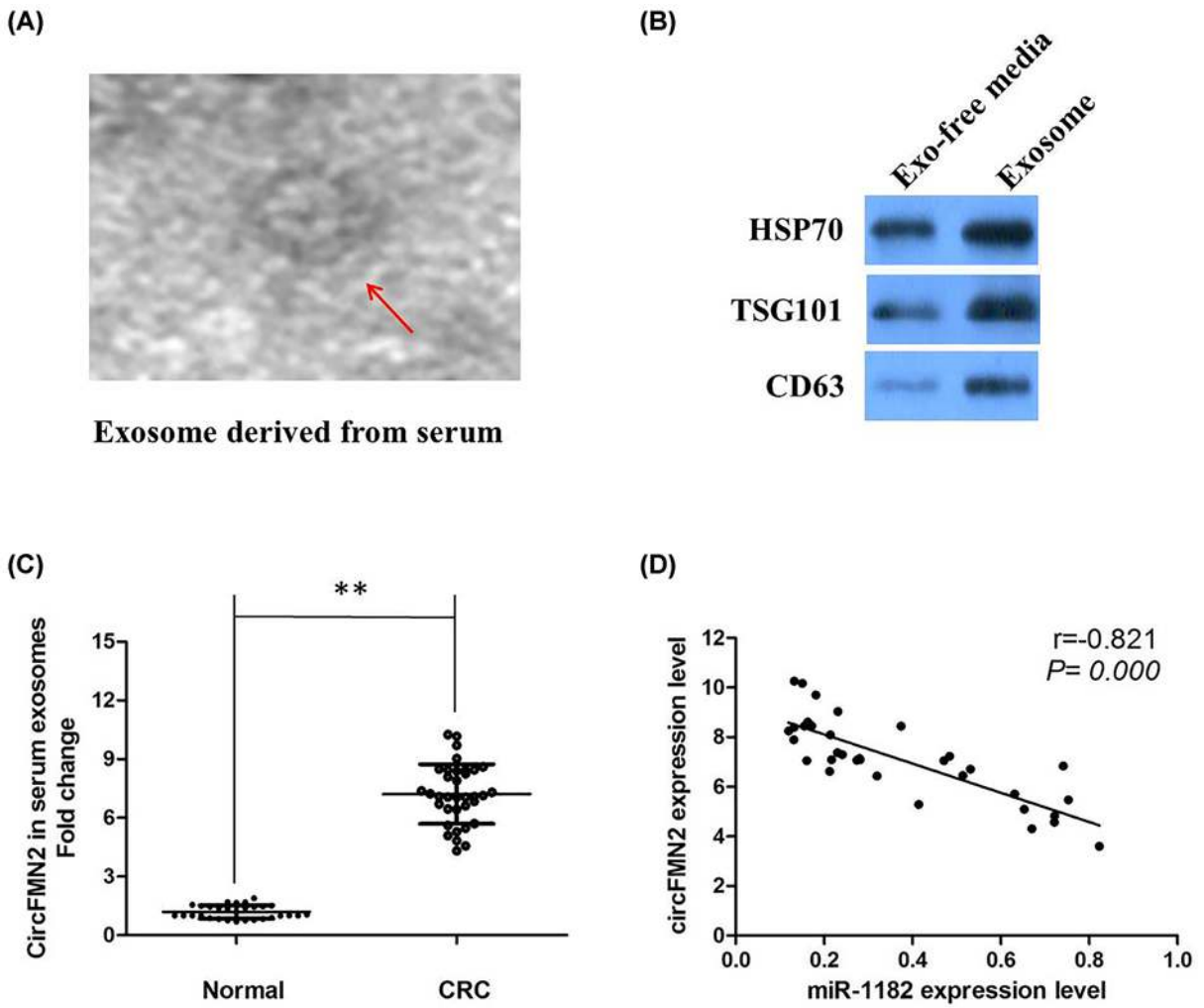

Figure 8. circFMN2 is secreted by exosomes into serum of CRC patients

(**A**) circFMN2 was secreted into exosomes derived from serum of CRC patients. A representative image of exosome (indicated by red arrows) derived from serum of CRC patients detected from electron microscope. (**B**) Western blot showing the expression of CD63, TSG101 and HSP70, which are the markers of exosome from purified serum exosome. (**C**) RT-qPCR for the abundance of circFMN2 in serum exosomes. The levels of circFMN2 in serum exosomes from CRC patients were significantly higher than that in normal individuals. (**D**) The expression levels of circFMN2 were negatively correlated with that of miR-1182 in the exosomes extracted from serum of CRC patients. All tests were at least performed three times. Data were expressed as mean ± SD; $^{**}P<0.01$.

functions. In this present study, we analyzed the expression profiles of circRNAs from CRC and matched non-tumor normal tissues by microarray, and focused on the role and underlying mechanism of the increased circFMN2 expression. Our findings report that circFMN2 expression is significantly elevated in CRC tissues and cell lines. Elevated expression of circFMN2 was positively correlated with correlated with larger tumor size, advanced tumor stage, distant metastasis, and TNM stage. We also discovered that circFMN2 exerted oncogenic function in the progression of CRC *in vitro* and *in vivo*. Functionally and mechanistically, circFMN2 promoted CRC progression by sponging miR-1182 and up-regulating hTERT expression. Finally, we showed that overexpressed circFMN2 was secreted by exosomes into the serum of CRC patients, suggesting that circFMN2 might be a novel clinical molecular marker for CRC patients. These results revealed that circFMN2 may act as a biomarker and therapeutic target for CRC.

Increasing evidence shows that circRNAs have a range of functions including regulation of RNA binding proteins (RBPs), promotion of mRNA transcription in *cis* and post-transcriptional regulation through sponging of miRNAs [26–28]. MiRNAs are a class of non-coding small RNAs of approximately 19–23 nucleotides in length, which are widely involved in various biological behaviors of cancer cells [29]. MiRNAs can post-transcriptionally reduce the

© 2019 The Author(s). This is an open access article published by Portland Press Limited on behalf of the Biochemical Society and distributed under the Creative Commons Attribution License 4.0 (CC BY-NC-ND).

Downloaded from http://portlandpress.com/clinsci/article-pdf/133/24/2463/864387/cs-2019-0715.pdf by guest on 20 August 2022

levels of specific target protein coding gene expression by binding to the 3′UTR of target mRNAs and resulting in translation inhibition or mRNA degradation. Studies showed that miRNAs are closely related to cell biological processes of CRC. Recently, miR-1182 has been reported as a tumor suppressor that is significantly down-regulated in multiple cancer types. We found that miR-1182 was expressed at a significantly lower level in CRC tumor tissues than in paratumor tissues. In our study, hTERT was predicted as the candidate target gene of miR-1182 by miRDB and TargetScan, and was further testified by dual-luciferase reporter assay. Next, we verified that circFMN2 had an endogenous sponge-like effect on miR-1182 in CRC. Furthermore, bioinformatics prediction and a luciferase reporter assay showed that circFMN2 and the hTERT 3′UTR share identical miR-1182 response elements and might therefore bind competitively to miR-1182. Third, circFMN2 could bind directly to miR-1182 in an AGO2-dependent manner. Finally, circFMN2 could control the hTERT level by provoking miR-1182. It has recently been reported that circRNAs can act as miRNA sponges to negatively control miRNA. The majority of circRNAs can function as sponges, via a mechanism of back-splicing, as they are enriched in miRNA binding sites. They can also competitively bind to miRNAs and decrease the activity of miRNAs. Our results further showed that circRNAs can serve as competitive endogenous RNAs and play an important role in CRC development.

Exosomes, derived from the endosomal compartment, are released in the extracellular milieu under various physiological and pathological conditions [30]. It has been reported that exosomes are closely related to tumor development, including angiogenesis, metastasis, drug resistance, and immune escape [31], but the role of cancer-secreted exosomal circRNAs in CRC has not been clarified yet. Here, we performed TEM to reveal the shapes and size of exosomes from serum of CRC patients. Notely, we found that the highly expressed circFMN2 could be examined to serum exosomes of CRC patients. We found that circFMN2 levels are negatively correlated with miR-1182 levels in CRC patients' serum.

Conclusions

In summary, our present study demonstrated that circFMN2 was up-regulated in CRC cell lines and tissues, and its high expression was associated with poor clinicopathological characteristics of CRC patients. Mechanistically, circFMN2 could significantly promote proliferation of CRC through directly binding to miR-1182 and subsequently reduce the suppressing capability of miR-1182 on hTERT. Exosome circFMN2 secreted from CRC patients' serum play an important role to promote the tumor growth of CRC. Our study suggested that circFMN2 was a novel potential biomarker and therapeutic target in CRC.

Clinical perspectives

- The molecular mechanisms that link circRNAs with CRC are not well understood.
- CircFMN2 was an oncogenic factor that promotes tumorigenesis by serving as a ceRNA to regulate hTERT expression by sponging miR-1182.
- CircFMN2 is a central component linking circRNAs to progression of CRC via an miR-1182/hTERT axis.

Funding

This study was approved by National Natural Science Foundation of China [grant number 81872323] and the Science and Technology Department of Jilin Province [grant number 20190303149SF].

Availability of Data and Materials

The datasets supporting the conclusions of this article are included within the article and its additional files.

Author Contribution

Changfeng Li performed primers design and experiments. Yongchao Li and Ruisi Xu contributed flow cytometry assay and animal experiments. Dandan Li and Bin Zhang collected and classified the human tissue samples. Yongchao Li and Ruisi Xu contributed to qRT-PCR. Changfeng Li and Yun Wang analyzed the data. Changfeng Li wrote the paper. All authors read and approved the final manuscript.

© 2019 The Author(s). This is an open access article published by Portland Press Limited on behalf of the Biochemical Society and distributed under the Creative Commons Attribution License 4.0 (CC BY-NC-ND).

Downloaded from http://portlandpress.com/clinsci/article-pdf/133/24/2463/864387/cs-2019-0715.pdf by guest on 20 August 2022

Clinical Science (2019) **133** 2463–2479
https://doi.org/10.1042/CS20190715

Ethics Approval and Consent to Participate

This study was approved by the Medical Ethics Committee of China-Japan Union Hospital of Jilin University.

Consent for Publication

We have received consent from the individual patients who have participated in the present study. The consent forms will be provided upon request.

Competing Interests

The authors declare that there are no competing interests associated with the manuscript.

Abbreviations

CCK-8, cell counting kit-8; ceRNA, competing endogenous RNA; circRNA, circular RNA; COAD, colon adenocarcinoma; CRC, colorectal cancer; FC, fold change; hTERT, human telomerase reverse transcriptase; IHC, immunohistochemistry; miRNA, microRNA; qRT-PCR, quantitative real-time PCR; PBS, phosphate-buffered saline; RIP, RNA immunoprecipitation; siRNA, small interfering RNA; TCGA, the Cancer Genome Atlas; TEM, transmission electron microscopy.

References

1 Siegel, R.L., Miller, K.D. and Jemal, A. (2018) Cancer statistics, 2018. *CA Cancer J. Clin.* **68**, 7–30, https://doi.org/10.3322/caac.21442
2 Bray, F., Ferlay, J., Soerjomataram, I., Siegel, R.L., Torre, L.A. and Jemal, A. (2018) Global cancer statistics 2018: GLOBOCAN estimates of incidence and mortality worldwide for 36 cancers in 185 countries. *CA Cancer J. Clin.* **68**, 394–424, https://doi.org/10.3322/caac.21492
3 Chen, W., Zheng, R., Zeng, H., Zhang, S. and He, J. (2015) Annual report on status of cancer in China, 2011. *Chin. J. Cancer Res.* **27**, 2–12
4 Colussi, D., Brandi, G., Bazzoli, F. and Ricciardiello, L. (2013) Molecular pathways involved in colorectal cancer: implications for disease behavior and prevention. *Int. J. Mol. Sci.* **14**, 16365–16385, https://doi.org/10.3390/ijms140816365
5 Memczak, S., Jens, M., Elefsinioti, A., Torti, F., Krueger, J., Rybak, A. et al. (2013) Circular RNAs are a large class of animal RNAs with regulatory potency. *Nature* **495**, 333–8, https://doi.org/10.1038/nature11928
6 Fan, X., Zhang, X., Wu, X., Guo, H., Hu, Y., Tang, F. et al. (2015) Single-cell RNA-seq transcriptome analysis of linear and circular RNAs in mouse preimplantation embryos. *Genome Biol.* **16**, 148, https://doi.org/10.1186/s13059-015-0706-1
7 Granados-Riveron, J.T. and Aquino-Jarquin, G. (2016) The complexity of the translation ability of circRNAs. *Biochim. Biophys. Acta* **1859**, 1245–51, https://doi.org/10.1016/j.bbagrm.2016.07.009
8 Wang, R., Zhang, S., Chen, X., Li, N., Li, J., Jia, R. et al. (2018) CircNT5E acts as a sponge of miR-422a to promote glioblastoma tumorigenesis. *Cancer Res.* **78**, 4812–4825, https://doi.org/10.1158/0008-5472.CAN-18-0532
9 Han, D., Li, J., Wang, H., Su, X., Hou, J., Gu, Y. et al. (2017) Circular RNA circMTO1 acts as the sponge of microRNA-9 to suppress hepatocellular carcinoma progression. *Hepatology* **66**, 1151–1164, https://doi.org/10.1002/hep.29270
10 Zhong, Z., Huang, M., Lv, M., He, Y., Duan, C., Zhang, L. et al. (2017) Circular RNA MYLK as a competing endogenous RNA promotes bladder cancer progression through modulating VEGFA/VEGFR2 signaling pathway. *Cancer Lett.* **403**, 305–317, https://doi.org/10.1016/j.canlet.2017.06.027
11 Barrett, S.P. and Salzman, J. (2016) Circular RNAs: analysis, expression and potential functions. *Development* **143**, 1838–47, https://doi.org/10.1242/dev.128074
12 Guo, J.U., Agarwal, V., Guo, H. and Bartel, D.P. (2014) Expanded identification and characterization of mammalian circular RNAs. *Genome Biol.* **15**, 409, https://doi.org/10.1186/s13059-014-0409-z
13 Li, Z., Huang, C., Bao, C., Chen, L., Lin, M., Wang, X. et al. (2015) Exon-intron circular RNAs regulate transcription in the nucleus. *Nat. Struct. Mol. Biol.* **22**, 256–64, https://doi.org/10.1038/nsmb.2959
14 Han, B., Chao, J. and Yao, H. (2018) Circular RNA and its mechanisms in disease: from the bench to the clinic. *Pharmacol. Ther.* **187**, 31–44, https://doi.org/10.1016/j.pharmthera.2018.01.010
15 Liu, J., Liu, T., Wang, X. and He, A. (2017) Circles reshaping the RNA world: from waste to treasure. *Mol. Cancer* **16**, 58, https://doi.org/10.1186/s12943-017-0630-y
16 Pan, B.T., Teng, K., Wu, C., Adam, M. and Johnstone, R.M. (1985) Electron microscopic evidence for externalization of the transferrin receptor in vesicular form in sheep reticulocytes. *J. Cell Biol.* **101**, 942–8, https://doi.org/10.1083/jcb.101.3.942
17 Li, Y. et al. (2015) Circular RNA is enriched and stable in exosomes: a promising biomarker for cancer diagnosis. *Cell Res.* **25**, 981–4, https://doi.org/10.1038/cr.2015.82
18 Zhang, H., Deng, T., Ge, S., Liu, Y., Bai, M., Zhu, K. et al. (2019) Exosome circRNA secreted from adipocytes promotes the growth of hepatocellular carcinoma by targeting deubiquitination-related USP7. *Oncogene* **38**, 2844–2859, https://doi.org/10.1038/s41388-018-0619-z
19 Zhang, D., Xiao, Y.F., Zhang, J.W., Xie, R., Hu, C.J., Tang, B. et al. (2015) miR-1182 attenuates gastric cancer proliferation and metastasis by targeting the open reading frame of hTERT. *Cancer Lett.* **360**, 151–9, https://doi.org/10.1016/j.canlet.2015.01.044
20 Xiao, J., Yu, H. and Ma, Z. (2019 Jun 6) LINC00339 promotes growth and invasiveness of hepatocellular carcinoma by the miR-1182/SKA1 pathway. *Onco Targets Ther.* **12**, 4481–4488, https://doi.org/10.2147/OTT.S207397
21 Zheng, L., Hu, N. and Zhou, X. (2019) CF3-activated LINC00152 exerts oncogenic role in osteosarcoma through regulating miR-1182/CDK14 axis. *Pathol. Res. Pract.* **215**, 373–380, https://doi.org/10.1016/j.prp.2018.12.031

© 2019 The Author(s). This is an open access article published by Portland Press Limited on behalf of the Biochemical Society and distributed under the Creative Commons Attribution License 4.0 (CC BY-NC-ND).

Downloaded from http://portlandpress.com/clinsci/article-pdf/133/24/2463/864387/cs-2019-0715.pdf by guest on 20 August 2022

22 Qu, S., Yang, X., Li, X., Wang, J., Gao, Y., Shang, R. et al. (2015) Circular RNA: a new star of noncoding RNAs. *Cancer Lett.* **365**, 141–148, https://doi.org/10.1016/j.canlet.2015.06.003
23 Salzman, J., Gawad, C., Wang, P.L., Lacayo, N. and Brown, P.O. (2012) Circular RNAs are the predominant transcript isoform from hundreds of human genes in diverse cell types. *PLoS ONE* **7**, e30733, https://doi.org/10.1371/journal.pone.0030733
24 Wang, R., Zhang, S., Chen, X., Li, N., Li, J., Jia, R. et al. (2018) CircNT5E acts as a sponge of microRNA-422a to promote glioblastoma tumorigenesis. *Cancer Res.*, https://doi.org/10.1158/0008-5472.CAN-18-0532
25 Liu, H., Liu, Y., Bian, Z., Zhang, J., Zhang, R., Chen, X. et al. (2018) Circular RNA YAP1 inhibits the proliferation and invasion of gastric cancer cells by regulating the miR-367-5p/p27 (Kip1) axis. *Mol. Cancer* **17**, 151, https://doi.org/10.1186/s12943-018-0902-1
26 Song, J., Wang, H.L., Song, K.H., Ding, Z.W., Wang, H.L., Ma, X.S. et al. (2018) CircularRNA_104670 plays a critical role in intervertebral disc degeneration by functioning as a ceRNA. *Exp. Mol. Med.* **50**, 94, https://doi.org/10.1038/s12276-018-0125-y
27 Su, H., Tao, T., Yang, Z., Kang, X., Zhang, X., Kang, D. et al. (2019) Circular RNA cTFRC acts as the sponge of MicroRNA-107 to promote bladder carcinoma progression. *Mol. Cancer* **18**, 27, https://doi.org/10.1186/s12943-019-0951-0
28 Yang, R., Xing, L., Zheng, X., Sun, Y., Wang, X. and Chen, J. (2019) The circRNA circAGFG1 acts as a sponge of miR-195-5p to promote triple-negative breast cancer progression through regulating CCNE1 expression. *Mol. Cancer* **18**, 4, https://doi.org/10.1186/s12943-018-0933-7
29 Ambros, V. (2004) The functions of animal microRNAs. *Nature* **431**, 350, https://doi.org/10.1038/nature02871
30 Thakur, B. K. et al. (2014) Double-stranded DNA in exosomes: a novel biomarker in cancer detection. *Cell Res.* **24**, 766–769, https://doi.org/10.1038/cr.2014.44
31 Dai, X. et al. (2018) Exosomal circRNA_100284 from arsenite-transformed cells, via microRNA-217 regulation of EZH2, is involved in the malignant transformation of human hepatic cells by accelerating the cell cycle and promoting cell proliferation. *Cell Death. Dis.* **9**, 454, https://doi.org/10.1038/s41419-018-0485-1

Downloaded from http://portlandpress.com/clinsci/article-pdf/133/24/2463/864387/cs-2019-0715.pdf by guest on 20 August 2022

© 2019 The Author(s). This is an open access article published by Portland Press Limited on behalf of the Biochemical Society and distributed under the Creative Commons Attribution License 4.0 (CC BY-NC-ND).